International Journal of Pavement Engineering
Publication details, including instructions for authors and subscription information:
http://www.tandfonline.com/loi/gpav20

Approximate simulation of storm water runoff over pervious pavement

Jiong Zhang[a], Xinzhuang Cui[a], Weize Tang[a] & Junjie Lou[a]
[a] School of Civil Engineering, Shandong University, Jinan, P.R. China
Published online: 24 Jul 2015.

To cite this article: Jiong Zhang, Xinzhuang Cui, Weize Tang & Junjie Lou (2015): Approximate simulation of storm water runoff over pervious pavement, International Journal of Pavement Engineering, DOI: 10.1080/10298436.2015.1065993

To link to this article: http://dx.doi.org/10.1080/10298436.2015.1065993

INTERNATIONAL JOURNAL OF PAVEMENT ENGINEERING, 2015
http://dx.doi.org/10.1080/10298436.2015.1065993

Taylor & Francis
Taylor & Francis Group

Approximate simulation of storm water runoff over pervious pavement

Jiong Zhang, Xinzhuang Cui, Weize Tang and Junjie Lou

School of Civil Engineering, Shandong University, Jinan, P.R. China

ABSTRACT

The approximate simulation of storm water run-off over pervious pavement is carried out using both experimental method and numerical simulation. The slope and flow rate changeable flume and uniform porous media are used to approximately simulate the pervious pavement. A 3D computational fluid dynamics – discrete element method is used for numerical simulation of interaction between pervious pavement and fluid. The effects of variation of parameters, including inflow rate, infiltration outflow rate and slope on surface run-off are analysed. The average flow velocity within the surface run-off region and shear velocity increases with the increasing permeability of pervious pavement. The turbulent kinetic energy distribution along depth in the free-flow region is more uniform than empirical relationship for flow over impermeable surfaces. Equations for flow depth and velocity over pervious pavement have been deduced. The results of this study are helpful for the hydraulic design of pervious concrete pavement.

ARTICLE HISTORY
Received 4 February 2015
Accepted 23 May 2015

KEYWORDS
Pervious pavement; storm water run-off; turbulent flow; approximate simulation; numerical simulation

1. Introduction

Pervious pavement also referred to as porous pavement, including pervious concrete pavement and OGFC (open graded friction course) pavement, has a large number of connected pores within the aggregate skeleton. The permeability is typically between 2 and 6 mm/s but can be as high as 10 mm/s (Tennis *et al.* 2004, Montes *et al.* 2005). The primary benefit offered by pervious pavement is the ability to transport large volumes of water through the material structure, thus reducing or eliminating problems associated with storm water run-off (Pratt *et al.* 1989, 1995, Newman *et al.* 2004, Collins *et al.* 2008). Other environmental benefits of pervious concrete pavement include the abilities to reduce tire–pavement interaction noise, and to limit the amount of organic and inorganic pollutants entering the groundwater (Kajio *et al.* 1998, Pratt *et al.* 2002, Neithalath 2004, Mulligan 2005, Coupe and Nnadi 2007, Nnadi *et al.* 2014b, 2015).

The design of a pervious pavement must consider many factors. The stress response, permeability, mix design and conservation methods of pervious concrete have been systematically studied. Alam *et al.* (2012, 2013) proposed a finite element model to simulate the stress and deformation behaviour of pervious concrete. Luck *et al.* (2006) showed the good draining capability of pervious concrete. Based on the Carman–Kozeny equation, Montes and Haselbach (2006) established a quantitative relationship between porosity and hydraulic conductivity of pervious concrete. Schluter and Jefferies (2002) studied the 20-month-old porous pavement in Edinburgh, and the result showed that porous pavement performed excellent outflow behaviour. Several researchers have used different methods of measuring the permeability of pervious pavement in the lab and field, (Cooley and Brown 2000, Maupin 2000, 2001, Prowell and Dudley 2002, Haselbach *et al.* 2006, Williams 2007, Kayhanian *et al.* 2012); majority of the field permeability measurements were performed using National Center for Asphalt Technology permeameter.

Experiments pointed out that the magnitude of storm water run-off has been greatly increased over impervious surfaces (Arnold and Gibbons 1996), and porous pavements can effectively reduce the run-off volumes (Rushton and Bahk 2001). Leming *et al.* (2007) provides an overview of hydrologic design techniques to limit the total surface run-off with the benefits of storage capacity of pervious concrete pavement system during the storm. Various parameters used in hydrologic models must be estimated based on experience assumptions, while the assumptions get uncertainty and variability involved.

A limited number of studies related to the hydraulic phenomenon of storm water run-off over pervious pavement have been reported. Illgen *et al.* (2007) represented a broad database and developed an approach for modelling run-off and infiltration processes of permeable pavements. Nnadi *et al.* (2014a) proposed an enhanced geotextile layer in permeable pavement to improve storm water infiltration. Sañudo-Fontaneda *et al.* (2014) analysed the infiltration performance of polymer-modified pervious surfaces and also quantified the infiltration capacity reduction due to clogging. However, additional research is needed on the effect of a permeable pavement on the turbulent run-off, the flow characteristics near the interface and the momentum transfer across the interface. Because these effects influence the depth and velocity of surface run-off, which will further influence sediment load carried by run-off.

CONTACT Xinzhuang Cui cuixz@sdu.edu.cn

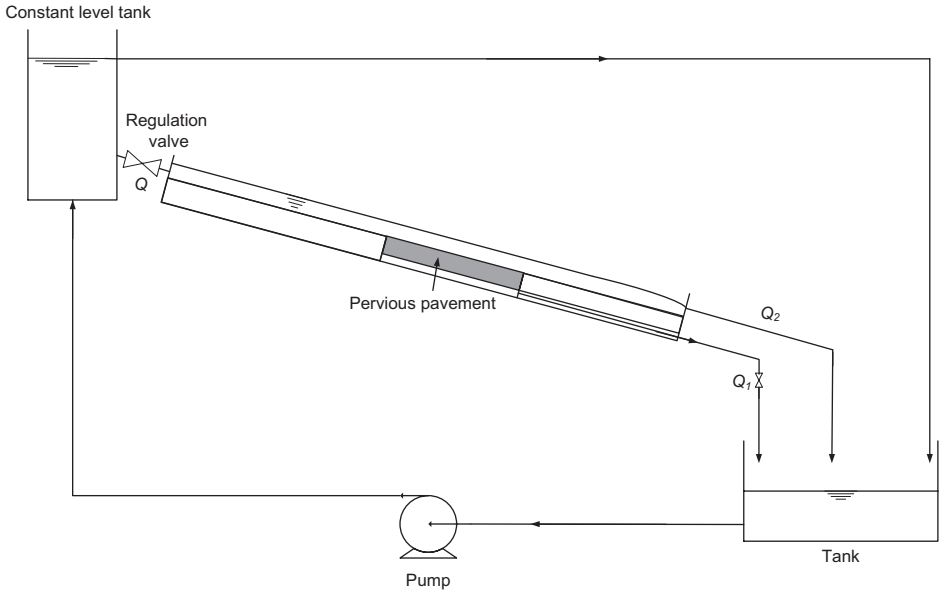

Figure 1. Sketch of storm water run-off over pervious pavement.

In this article, the storm water run-off over pervious pavement is approximately simulated (Figure 1). The effects of variation of parameters, including inflow rate, infiltration outflow rate and slope on surface run-off, are analysed using both experimental and numerical methods. The flume which can change slope and flow rate and uniform porous media are used to approximately simulate the pervious pavement. With this approximate experimental method, the parameters can be well controlled in a particular case study, and uncertainties which influence the results can be avoided. At the same time, numerical fluid–solid interaction method (ITASCA 2008) was used to obtain the flow velocity field inside the pervious pavement and mutually verify with the experimental velocity field in the free surface flow. The turbulent kinetic energy transfer across the interface is also quantitatively analysed by experiments and numerical simulation. The aim of this study was to provide a detailed view of how the storm water will actually be conveyed over pervious pavement, and to deduce equations for flow depth and velocity over pervious pavement, therefore the research results can promote the hydraulic design of pervious pavement.

2. Experimental set-up and procedure

2.1. Flume and porous pavement

A laboratory experiment was carried out in a circulating flume of 200 cm long, 3 cm wide and 8.5 cm deep. The flume is made up by Plexiglas entirely, which can provide a good view from both sides. It is based on a smooth marble surface and supported by an adjustable steel structure which gives the ability to change the slope with an electric motor. Water is pumped into a constant level tank, and then goes to the entrance of the flume. There are device sites at the entrance portion of the flume intend to reduce turbulences, bubbles, etc. because of the sudden change of section. This device is made up by an array of straws with a diameter of 5 mm and a length of 10 cm. A schematic diagram of the experiment system used in this study is shown in Figure 2.

The approximate model of the pervious concrete pavement system is installed at 100 cm from flume upstream end. Its structure is shown in Figure 3. A model porous pavement is made up by the aggregates of magnetic stainless steel balls. There are several advantages of this kind of balls, such as, they could be used to compose the porous media with different porosity without any

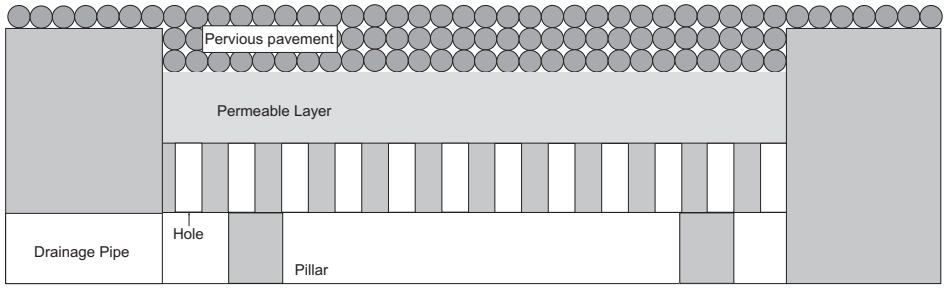

Figure 2. Experiment system scheme (***Q***: total flow rate, $\boldsymbol{Q}_1$: water flowing through the sample and $\boldsymbol{Q}_2$: water flowing over the sample).

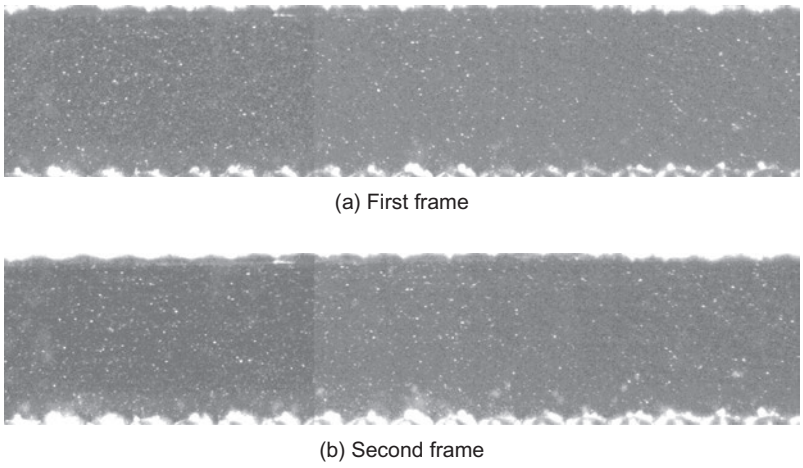

Figure 3. Approximate model of the pervious concrete pavement system.

glue, so they could be disassembled and reused, the precision of diameter is very good and the magnetic force between the balls is big enough to protect the structure of porous media counter the flow. Spherical particles of equal size theoretically may be packed in five different ways (White and Walton, 1937). In our study, a cubic pack (with porosity of 47.64%) with 2010 pieces of 3-mm magnetic stainless steel balls is employed, and the size of porous pavement is 201 mm × 30 mm × 9 mm. The appearance of this thin porous medium can simulate the interface of fluid flow and upper part of pervious concrete pavement with a large number of pores, where the coupled phenomenon can take place such as turbulent kinetic energy penetrates from the surface flow to the upper part of pervious pavement. Under the porous pavement is a permeable layer in synthetic felt. The third layer is a plastic board with holes. There are pillars to support all these layers, and at the end of the void layer, a pipe is used to drain the infiltrated water outside of the flume. Outside of the study zone, plastic boards with a single layer of magnetic balls spread on it are used to level up the bottom of the flume to the same level of the porous pavement.

As one can see from Figure 3, this experimental set-up is an approximate simulation of a tiny part taken from the real storm water run-off over pervious pavement (as shown in Figure 1), although some details are idealised and the influence of precipitation on this tiny surface are also ignored. The purpose of employing this approximate model of the pervious pavement instead using a real pervious concrete block is to avoid the randomness of complex pore structure of pervious concrete specimens. Even specimens with the same porosity, the inside pore networks and surface characteristics could be randomly different, also in reality, there are a few unconnected pores in the specimen (Alam and Haselbach 2014). All these uncertainties can have important influences on the results.

To control the total flow rate in the flume and the infiltration flow rate through the porous pavement, an electronic balance and a tank were placed at the end of the flume. The water will be received entirely by this tank during the measurement and the electronic balance placed under this tank connected with computer can give a mass change record of the tank every second, so the volume flow rate Q in unit of l/min is then calculated. The repeatability of the electronic balance is 0.01 g. The high precision is the primary advantage of this measure method.

2.2. Measure of the flow velocity field by a particle image velocimetry (PIV) system

After the flow in the model became steady and established, a PIV system made by Dantec dynamics was used to measure the instantaneous two-dimensional velocity fields. A PIV system typically consists of a laser with sheet optics, one digital camera, and a computer with a timer unit to control the system and store the data. An acquisition corresponding to 100 double-frame images is employed, the interval time between every capture is 1000 μs and the time between the two frames of a double-frame is 500 μs. The size of the particles is about 50 μm.

An example of a double-frame image for PIV computation (flow condition: inflow rate Q = 6 l/min and slope S_o = 0.0105) is given in Figure 4.

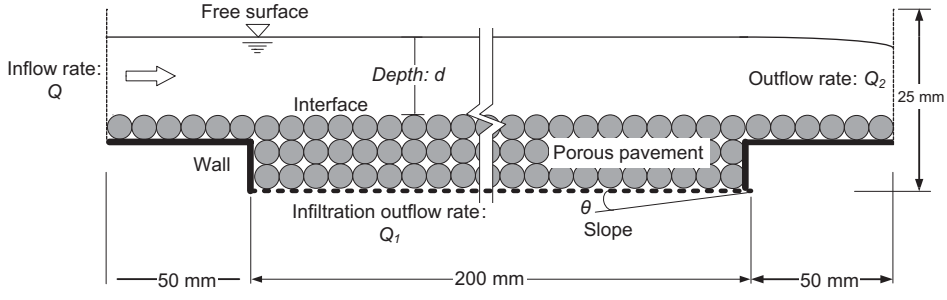

Figure 4. A double-frame image for PIV computation.

2.3. Experimental procedure

(1) The slope of flume is adjusted by a motor.
(2) Turn on the pump and fill constant level tank with water, use the regulation valve and electronic balance to adjust the inflow rate and the infiltration outflow rate.
(3) After the flow is steady, the flow velocity field is measured with a PIV system.
(4) Change the parameters, such as slope, inflow rate, and infiltration outflow rate, etc. and repeat the steps (1)–(3).

2.4. Test cases

Three parameters have been studied in this work: slope, inflow rate and infiltration outflow rate. Totally, 28 cases were studied by both experiments and numerical simulations. The porosity of the porous pavement remains fixed to the value of 0.476 for all cases.

(1) A range of four slopes (S_o) were chosen for testing and they were: 0.0035, 0.0105, 0.0175 and 0.0244.
(2) Four inflow rates (Q) were chosen for testing: 3.20, 4.50, 6.00 and 6.80 l/min. They can create velocities between 0.2 and 0.5 m/s, and the storm water run-off velocity usually lies within the range.
(3) Four infiltration outflow rate (Q_1) were chosen for testing: 0, 5, 6.7 and 10% of the inflow rate (Q). As Darcy's law indicated, the change of infiltration outflow rate using valve is equivalent to the change of permeability of pervious pavement. The permeability between 0.0004 and 0.002 m/s can be obtained with the chosen values, and permeability of pervious concrete pavement typically lies within the range.

3. Numerical simulation

The computational fluid dynamics (CFD)–discrete element method (DEM) is used to obtain the flow velocity field inside the pervious pavement and mutually verify with the experimental velocity field in the free surface flow for each case.

In the CFD–DEM model (ITASCA 2008), the flow in the whole flow region is calculated from the continuity and the Navier-Stokes equations with a porosity term and an additional body force term to account for the presence of particles in the fluid, which are given by

$$\frac{\partial \Phi}{\partial t} + \nabla \cdot (\Phi \vec{u}) = 0 \tag{1}$$

$$\frac{\partial(\rho \Phi \vec{u})}{\partial t} + \nabla \cdot (\rho \Phi \vec{u}\vec{u}) = -\nabla p + \mu \nabla^2 (\Phi \vec{u}) - \vec{f}_b + \rho \Phi \vec{g} \tag{2}$$

where ρ is the density of the fluid, Φ is porosity, $\vec{u}$ is the fluid velocity, p is the fluid pressure, μ is the dynamic viscosity of the fluid, $\vec{f}_b$ is the body force per unit volume, $\vec{f}_b = \sum_{i=1}^{n_v} \vec{f}_{\text{fluid},i}$, where $\vec{f}_{\text{fluid},i}$ is the total force applied by the fluid on the particle i, n_v is the number of particles per unit volume and $\vec{g}$ is the gravitational acceleration. The porosity and body force in these fluid elements are determined by the DEM.

The equations of motion for particles with an additional force term to account for interaction with the fluid are expressed as:

$$m\frac{\partial \vec{u}_p}{\partial t} = \vec{f}_{\text{mech},i} + \vec{f}_{\text{fluid},i} + m\vec{g} \tag{3}$$

$$\frac{\partial \vec{\omega}}{\partial t} = \frac{\vec{M}}{I} \tag{4}$$

where $\vec{u}_p$ is the particle velocity, m is the particle mass, $\vec{f}_{\text{mech},i}$ is the sum of additional forces acting on the particle, $\vec{g}$ is the gravitational acceleration, $\vec{\omega}$ is the particle angular velocity, I is the moment of inertia and $\vec{M}$ is the moment acting on the particle.

$\vec{f}_{\text{fluid},i}$, the total force applied by the fluid on the particle i is made up of two parts: the drag force and a force due to the fluid pressure gradient, other particle-fluid forces, such as lift force can be ignored in this study:

$$\vec{f}_{\text{fluid},i} = \vec{f}_{\text{drag},i} + \frac{3}{4}\pi r^3 \nabla p \tag{5}$$

$$\vec{f}_{\text{drag},i} = \left(0.63 + \frac{4.8}{\sqrt{Re_{p,i}}}\right)^2 \left(\frac{1}{2}\rho\pi r_i^2 |\vec{u} - \vec{u}_{p,i}|\left(\vec{u} - \vec{u}_{p,i}\right)\right)\Phi^{-\chi} \tag{6}$$

where $\Phi^{-\chi}$ term is an empirical factor to account for the local porosity. This correction term makes the force applicable to both fixed and fluidised porosity systems and for a large range of Reynolds numbers (Di Felice 1994, Xu and Yu 1997).

The particle Reynolds number, Re_p is:

$$Re_{p,i} = \frac{d_{s,i}\rho|\vec{u} - \vec{u}_{p,i}|}{\mu} \tag{7}$$

The empirical coefficient χ is defined as:

$$\chi = 3.7 - 0.65 \exp\left[-\frac{(1.5 - \log_{10} Re_{p,i})^2}{2}\right] \tag{8}$$

DEM and CFD coupling is numerically achieved as follows: Equations (1) and (2) are solved with the CFD code (i.e. CCFD), and Equations (3) and (4) are solved with the DEM code (i.e. PFC3D). The porosity and the body force are determined in DEM and divided by volume in CFD. The fluid velocity and fluid pressure in every element are determined by CFD and send to DEM in each coupling data exchange. The volume of fluid method is used for tracking the position of the free surface.

Figure 5 shows the computational domain investigated here. The rectangular flume is partially filled with a layer of a porous pavement. A free surface flow passes longitudinally from left to right.

The computational domain has dimensions equal to 0.30 m (length) × 0.025 m (height) × 0.03 m (width), and the solution is based on a hexahedral mesh with mesh size of 1 mm × 0.5 mm × 1 mm. Fixed solid particles with a diameter of 3 mm are used as aggregates to assemble the pervious pavement. The thickness of the pervious pavement is 9 mm. The inlet flow depth is 8 mm. The computational time-step for CFD is chosen as 2.5×10^{-4} s, and the time-step for DEM is 5.0×10^{-5} s.

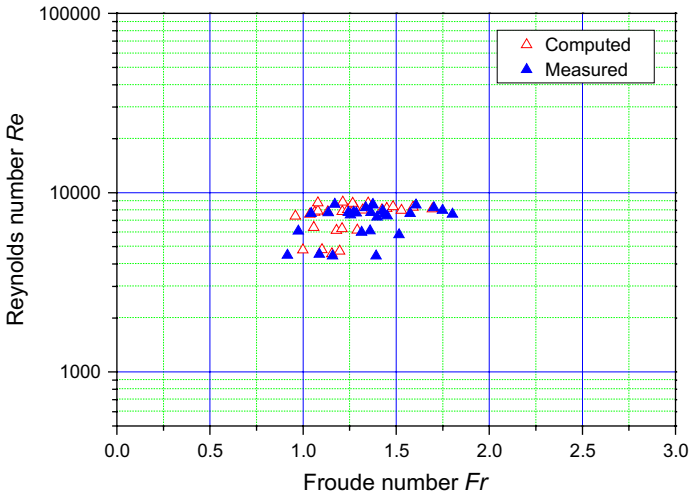

Figure 5. Sketch of computational domain with boundary conditions in a 2D view.

4. Results and discussion

4.1. Flow regimes

The flow of water is described by several complementary characterisations: steady and unsteady, uniform and non-uniform, laminar and turbulent, and supercritical and subcritical. Figure 6 shows the Reynolds number (*Re*) and Froude number (*Fr*) of the run-offs, these values are taken after the flow is steady. Because the maximum downward infiltration velocity is less than 1% of the mean run-off flow velocity, so the flow can be considered as uniform flow. *Fr* is between 0.9 and 1.6, while *Re* is between 4000 and 9000. Therefore, the run-offs are near-critical (i.e. $0.7 < Fr < 1.5$) or supercritical turbulent flows, i.e. the inertial force is dominant comparing with gravity force and viscous force in these surface run-offs.

4.2. Velocity distributions above and within the porous pavement

4.2.1. Influence of slope

Figure 7 presents the corresponding variation of the computed and measured velocity profiles for different slopes, in different infiltration conditions. There are small differences in velocities between computed and measured data, but that is in the range of tolerance. Evidently, the greater slope causes a higher flow velocity around the fluid/pavement interface and within fluid region, and the increases of infiltration outflow also cause relative higher flow velocity.

Measurements of the velocity within the pervious pavement cannot be easily performed by experiments, but the numerical simulation has the advantage that the velocity inside the porous medium could be known as well. Results show that the velocity profiles of different cases become separated from 1.5 mm (radius of aggregate) beneath the pervious pavement surface; this is because the pore size becomes larger from that position. In the deeper part of the pervious pavement, the seepage flow velocity is negligible compared with surface flow.

From Figure 7, the variation of flow depth with different slopes and infiltration outflow rates can also be found. As expected, both experimental and simulation flow depth lowered with higher slope. With the same slope flow depth slightly decreases when the infiltration outflow rate Q_1 increases.

So during pervious pavement design, the flatter slope ($S_o \le 0.0175$) should be used, which can effectively reduce the storm water run-off velocity. Smaller surface layer porosity of pervious pavement is also useful to reduce run-off velocity.

4.2.2. Influence of flow rate

Figure 8 shows the corresponding variation of velocity profiles for different flow rates. Either experimental or simulation velocities significantly augment with higher inlet flow rates. The variation tendency of flow depth with different inflow rates can also be found from these figures, depth goes up when inflow rate increases.

4.3. Shear velocity

The shear velocity is used to measure shear stress and velocity gradient near the boundary, a large shear velocity U_* implies large shear stress and large velocity gradient, and hence larger shear velocity will increase sediment load carried by the run-off.

Generally, there are four methods to estimate the shear velocity: Reynolds stress, logarithmic law, parabolic law and a global approach.

The simplest one, derived for steady uniform flow in wide channels, estimates U_* as:

$$U_* = \sqrt{g\frac{D_H}{4}S_o} \tag{9}$$

where g is the gravitational acceleration, D_H is the hydraulic diameter and S_o is the slope of the channel bed (for uniform flow the slope of the channel bed, the friction slope and the water-surface slope are all equal). In the case of steady non-uniform flow, the energy slope replaces S_o. In this study, the infiltration outflow rate would influence the energy slope. So accurate estimation of U_* by this method is difficult, therefore, U_* must be estimated with other methods.

The logarithmic law method is based on the velocity distribution in the region within $y/d < 0.6$ (where y is the distance to the bottom and d is the flow depth), can be described by the logarithmic law:

$$\frac{u}{U_*} = \frac{1}{\kappa}\ln\left(\frac{y}{k_s}\right) + C \tag{10}$$

where κ is the von Karman constant (equal to 0.41) and C is a constant. Einstein and El-Samni (1949) proposed a modified logarithmic law for the flow over a surface with large roughness:

$$\frac{u}{U_*} = \frac{1}{\kappa}\ln\left(\frac{y+y_0}{k_s}\right) + C \tag{11}$$

where y_0 is the distance of the theoretical wall below the top of the spheres whose diameter is k_s, (Figure 9), they chose a value of $y_0 = 0.2k_s$.

Velocity profiles against $\ln y$ are plotted in Figures 10–12 to derive shear velocity U_*. In this study, the value of U_* is estimated from the slope of fitted line of velocity profiles to the

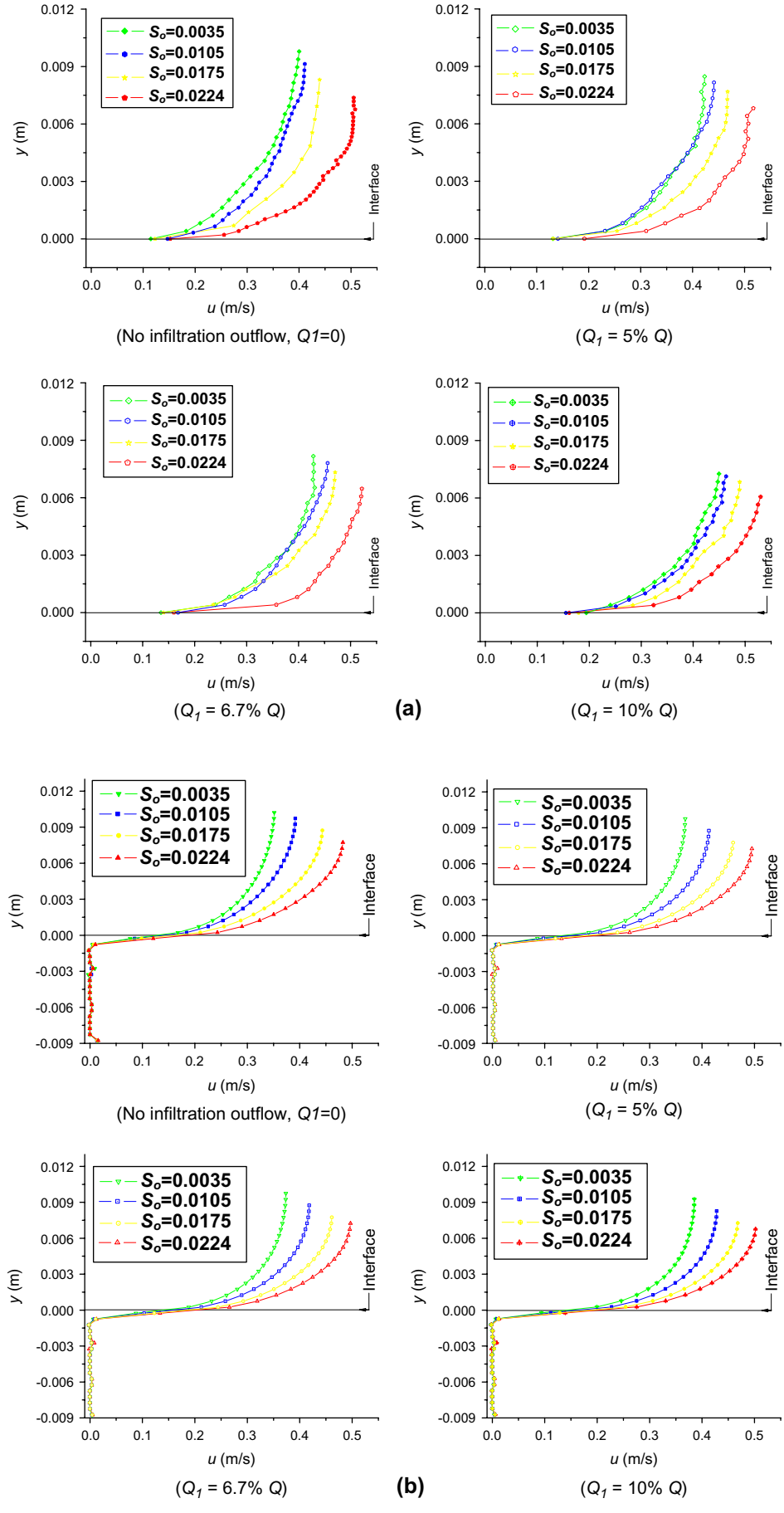

Figure 6. Reynolds number–Froude number of the surface run-offs.

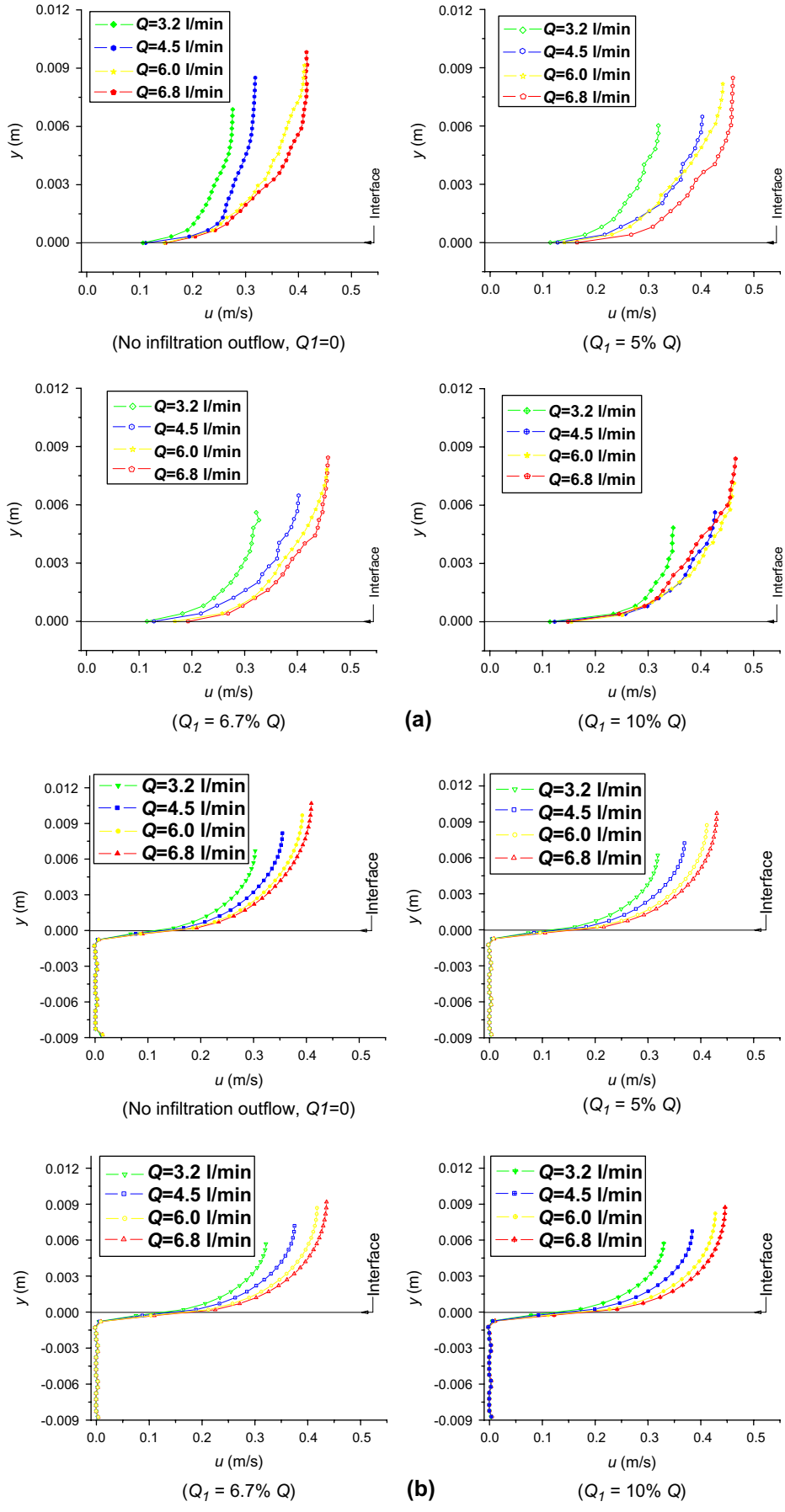

Figure 7. Flow velocity profiles above and within the pervious pavement for different slopes, in different infiltration conditions. (a) Measured data; (b) Simulated data.

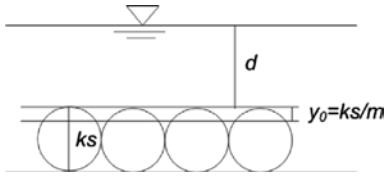

Figure 8. Flow velocity profiles above and within the porous region for different inflow rates, with different infiltration rates. (a) Measured data; (b) Simulated data.

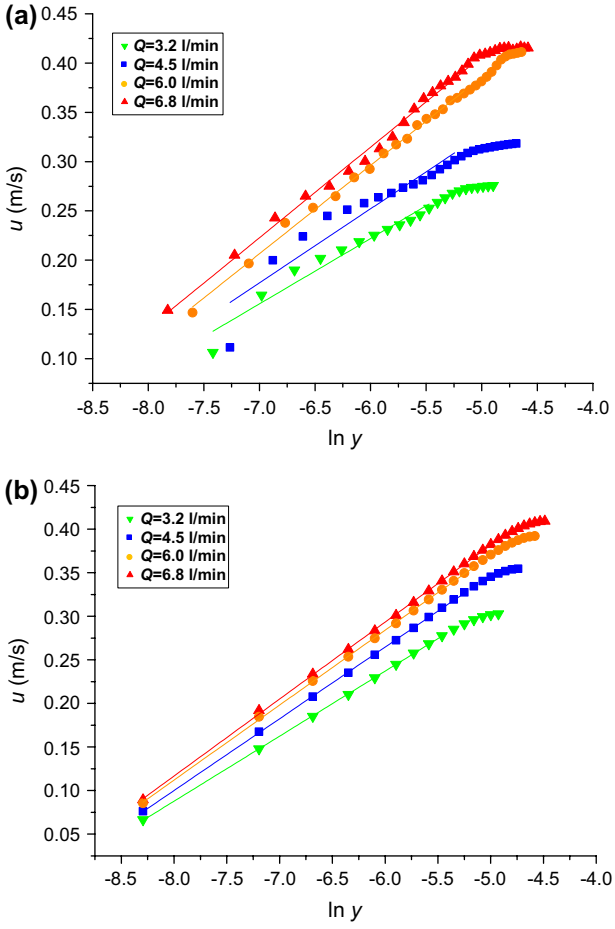

Figure 9. The position of y_0.

logarithmic law proposed by Einstein and El-Samni (1949). As the figures show that the modified logarithmic law proposed by Einstein and El-Samni (1949) is a convenient and accurate method to calculate shear velocity.

As shown in figures, shear velocity increases as inflow rate, slope and infiltration outflow rate increase.

4.4. Turbulent kinetic energy above and within the pervious pavement

The prediction of sediment load transport by storm water run-off depends on the turbulence model used in the bottom boundary layer over the pavement. Elliot and Trowsdale (2007) compared ten existing storm water models. Kim and Sansalone (2008) examined the particle size distributions of solid sediments transported by rainfall run-off, and provided a mass balance analysis to ensure representative event-based results.

The mechanism of turbulence is complicated. In the turbulent bottom boundary layer, the turbulent mixing motion

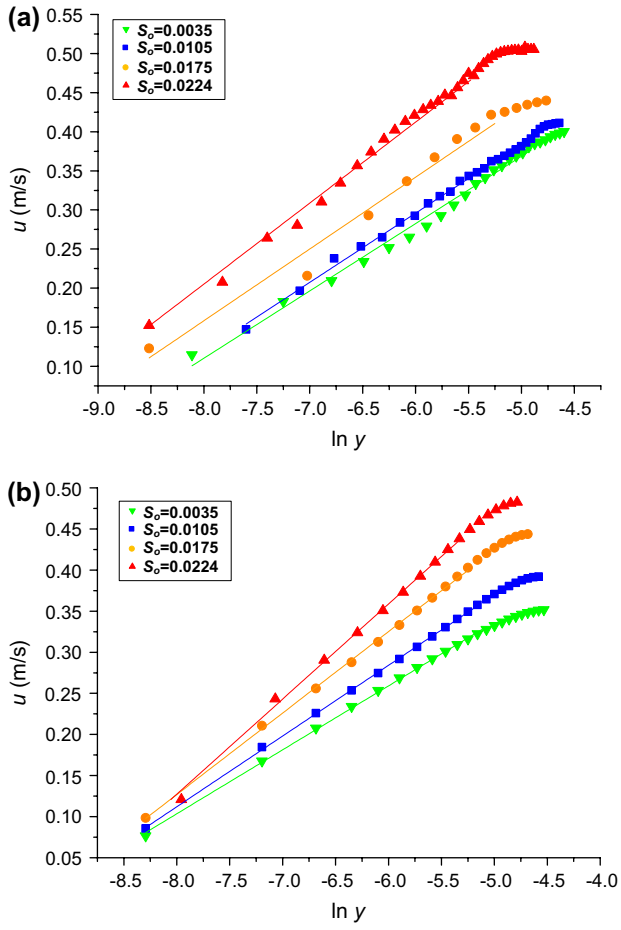

Figure 10. Velocity profiles against ln y for different inflow rates (slope S_o = 0.0105, without infiltration outflow). (a) Experimental results; (b) Computed results.

is responsible for an exchange of momentum, and it enhances the transfer of mass. In this article, the turbulent kinetic energy above and within the pervious pavement is studied numerically. Turbulence kinetic energy (k) is the mean kinetic energy per unit mass associated with eddies in turbulent flow. It can be quantified by the mean of the turbulence normal stresses.

Figure 13 presents the effect of slope on the normalised turbulent kinetic energy k^+ (= k/U_*^2). Figure 14 shows the normalised turbulent kinetic energy k^+ profiles of the fully developed flow for inflow rate Q varying from 3.2 to 6.8 l/min, with the infiltration outflow rate Q_1 varying from 0 to 10% Q for each inflow rate, and the slope is fixed to 0.0105.

After normalisation, little differences can be found. The value of k^+ increases rapidly in the y direction and reach to the maximum value in the region around the interface of free flow and pervious pavement, and then it decreases slowly in the surface flow region.

It is shown that the k^+ distribution in the free-flow region is more uniform than empirical relationship for flow over impermeable surfaces developed by Nezu and Nakagawa (1993), $k^+ = 4.78\exp(-2y/d)$. The empirical relationship for the range of these simulations is $k^+ = 2.97\exp(-2y/d)$. This is due to the penetration of turbulence to the upper part of pervious pavement in significant levels. Therefore, pervious pavement reduces the run-off turbulence in the bottom boundary layer, reduces the skin friction coefficient and hence increases the flow velocity.

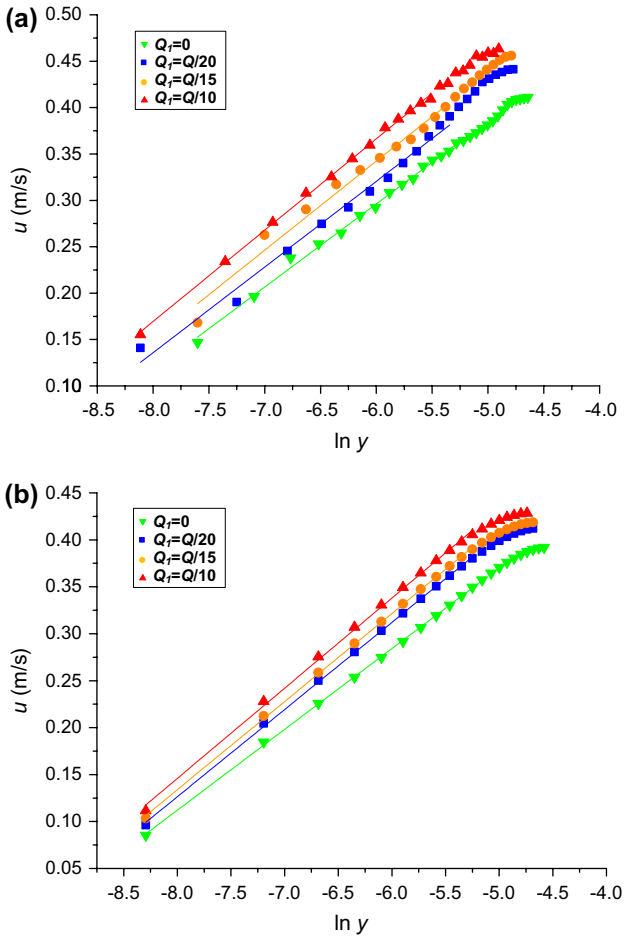

Figure 11 Velocity profiles against ln ***y*** for different slopes (inflow rate ***Q*** = 6.0 l/min, without infiltration outflow). (a) Experimental results; (b) Computed results.

4.5. Equations for flow depth and velocity

Storm water run-off on pervious concrete pavement surface and in partially infiltrated underground can be described mathematically by equations combining the shallow water equations for the surface flow and the Darcy's law for infiltration flow.

$$\frac{\partial q}{l} + \frac{\partial d}{t} = I\cos\vartheta - \frac{q_1}{l} \tag{12}$$

$$q = \frac{1}{n} S_o^{1/2} d^{5/3} \tag{13}$$

$$q_1 = kJl \tag{14}$$

where q is the flow rate per unit width; l is the length of pervious pavement; t is time; I is the rainfall intensity; θ is the angle between the pervious pavement and the horizontal; q_1 is the infiltration flow rate per unit width; n is the Manning coefficient; k is the permeability of pervious pavement; J is the hydraulic gradient. The first equation is the equation of continuity, the second the momentum equation and the third the Darcy's law.

The change of flow depth and velocity of surface run-off during a storm event is the most important parameter concerned by pervious pavement designers and operators. Therefore, Equations (12)–(14) can be rewritten as follows:

$$d_1 = [nS_o^{-1/2}(q_0 - kl)]^{3/5} \tag{15}$$

$$u_1 = n^{-3/5} S_o^{3/10} (q_0 - kl)^{2/5} \tag{16}$$

where d_1 and u_1 are the downstream flow depth and velocity of surface run-off flow over a pervious pavement with length of l, slope of S_o, Manning coefficient n and permeability of k; q_0 is the inflow rate per unit width of upstream boundary. With Equations (15) and (16), the change of depth and velocity over pervious pavement can be calculated conveniently. Note that the calculations are sensitive upon the choice of Manning coefficient, experimental investigations should be performed to estimate for each flow condition. In this study, $0.008 < n < 0.014$. With the estimated Manning coefficient, flow depths and velocities are calculated using Equations (15) and (16). Figure 15 shows that the results obtained from equations fit well with measured data.

5. Conclusions

The approximate simulation of storm water run-off over pervious pavement is carried out using both experimental method and numerical simulation. The flume which can change slope and flow rate and uniform porous media is used to approximately simulate the pervious pavement. Meanwhile, a numerical method was conducted using the CFD–DEM two-way coupling method to obtain the flow velocity field inside the pervious pavement. Surface turbulent run-off over pervious pavement has been studied for slope S_0 varied from 0.0035 to 0.0244, inflow rate Q varied from 3.2 to 6.8 l/min and infiltration outflow rate varied from 0 to 10% of the inflow rate. The following conclusions can be derived:

(1) The flow depth increases with increasing inflow rate and it decreases with increasing slope; simultaneously, the average flow velocity within the free-fluid region increases with increasing slope and inflow rate. The increases of infiltration outflow reduce the flow depth and cause relative higher flow velocity. Thus, the flatter slope can effectively reduce the storm water run-off velocity. Smaller surface layer porosity of pervious pavement is also useful to reduce run-off velocity.
(2) The shear velocity increases as slope and inflow rate increase.
(3) The normalised turbulent kinetic energy k^+ distribution in the surface run-off region is more uniform than empirical relationship for flow over impermeable surfaces. This is due to the penetration of turbulence to the upper part of pervious pavement in significant levels.

The approximate experimental method gives an idea of presenting the hydraulic phenomena taking place around the interface. Additional research based on this approximate simulation would be beneficial in creating an optimal design methodology. Influences of porosity of pervious concrete and higher slopes will be further investigated using pervious concrete specimens.

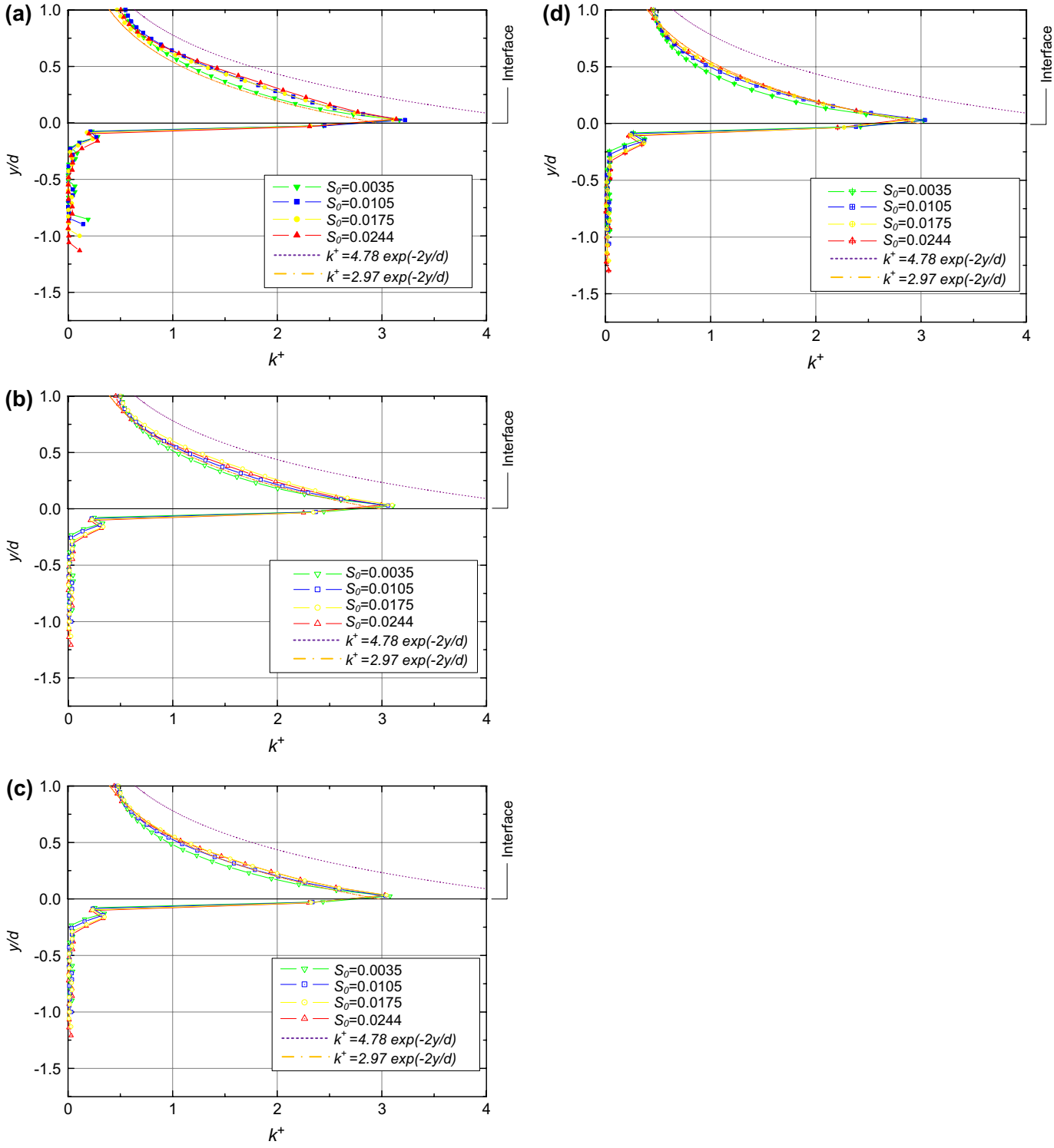

Figure 12. Velocity profiles against ln ***y*** for different infiltration outflow rates (inflow rate $\boldsymbol{Q}$ = 6.0 l/min, slope $\boldsymbol{S_o}$ = 0.0105). (a) Experimental results; (b) Computed results.

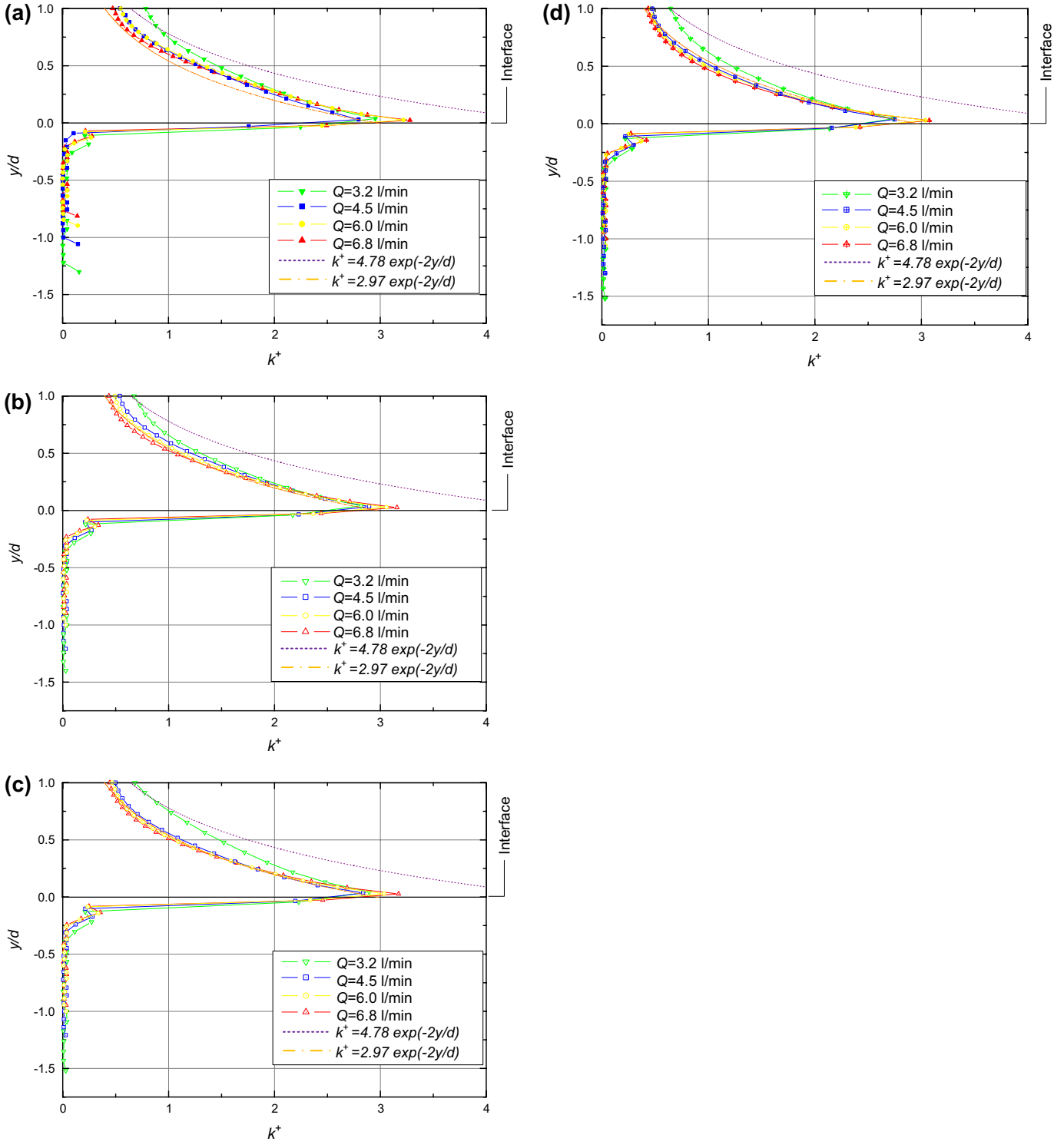

Figure 13. Variation of k/U_*^2 above and within pervious road for different slopes. (a) inflow rate $Q = 6$ l/min, no infiltration outflow rate; (b) inflow rate $Q = 6$ l/min, infiltration outflow rate $Q_1 = 0.3$ l/min; (c) inflow rate $Q = 6$ l/min, infiltration outflow rate $Q_1 = 0.4$ l/min; (d) inflow rate $Q = 6$ l/min, infiltration outflow rate $Q_1 = 0.6$ l/min.

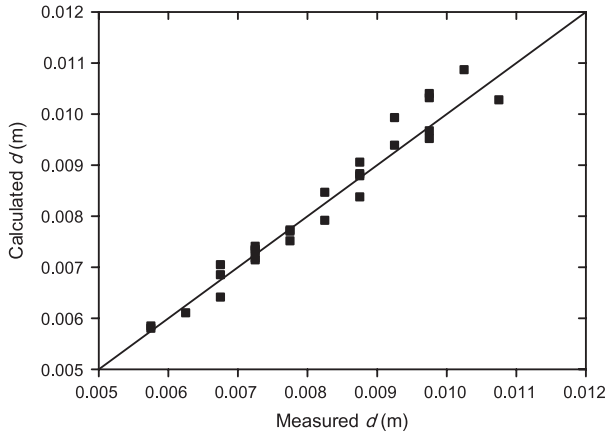

Figure 14. Variation of k/U_*^2 above and within pervious road for different inflow rates. (a) no infiltration outflow rate; (b) infiltration outflow rate Q_1 = 5% Q; (c) infiltration outflow rate Q_1 = 6.7% Q; (d) infiltration outflow rate Q_1 = 10% Q.

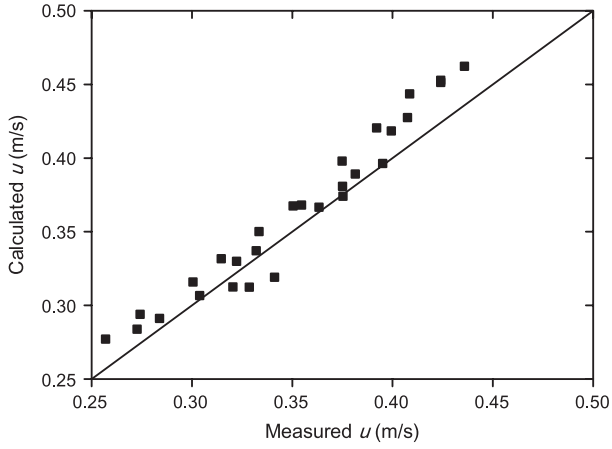

Figure 15. Verification of equations for flow depth and velocity. (a) flow depth; (b) flow velocity.

Disclosure statement

No potential conflict of interest was reported by the authors.

References

Alam, A. and Haselbach, L., 2014. Estimating the modulus of elasticity of pervious concrete based on porosity. *Advances in Civil Engineering Materials*, 3 (1), 256–269.

Alam, A., Haselbach, L., and Cofer, W., 2012. Validation of the performance of pervious concrete in a field application with finite element analysis. *Journal of ASTM International*, 9 (4), 1–16.

Alam, A., Haselbach, L., and Cofer, W., 2013. Three-dimensional finite element modeling and analysis of pervious concrete pavement: modified vertical porosity distribution approach. *International Journal of Research in Engineering and Technology*, 2 (12), 767–777.

Arnold, C. and Gibbons, J., 1996. Impervious surface coverage: the emergence of a key environmental indicator. *Journal of the American Planning Association*, 62, 243–258.

Collins, K., Hunt, W., and Hathaway, J., 2008. Hydrologic comparison of four types of permeable pavement and standard asphalt in eastern North Carolina. *Journal of Hydrologic Engineering*, 13 (12), 1146–1157.

Cooley, L.A. and Brown, E.R., 2000. Selection and evaluation of field permeability device for asphalt pavements. *Transportation Research Record: Journal of the Transportation Research Board*, 1723, 73–82.

Coupe, S.J. and Nnadi, E.O., 2007. Water recycling and ground source heat pump systems within permeable paving–system installation and on-site construction considerations. *In: National conference for sustainable urban drainage network (SUDSNET)*. Coventry: Coventry University.

Di Felice, R., 1994. The voidage function for fluid-particle interaction systems. *International Journal of Multiphase Flow*, 20, 153–159.

Einstein, H.A. and El-Samni, E.A., 1949. Hydrodynamic forces on a rough wall. *Reviews of Modern Physics*, 21, 520–524.

Elliot and Trowsdale, 2007. A review of models for low impact urban stormwater drainage. *Environmental Modelling & Software*, 22, (3), March 2007, 394–405.

Haselbach, L., Valavala, S., and Montes, F., 2006. Permeability predictions for sand-clogged Portland cement pervious concrete pavement systems. *Journal of Environmental Management*, 81 (1), 42–49.

Illgen, M., *et al.*, 2007. Runoff and Infiltration characteristics of permeable pavements – Review of an intensive monitoring program. *NOVATECH 2007*. Lyon.

ITASCA Consulting Group, Inc., 2008. *PFC3D 4.0 User Guide CCFD add-on*, Minneapolis, MN: Itasca Consulting Group Inc.

Kajio, S., *et al.*, 1998. Properties of porous concrete with high strength. *In*: *Proceedings 8th international symposium on concrete roads*. Lisbon: World Road Association (PIARC), 171–177.

Kayhanian, M., *et al.*, 2012. Permeability measurement and scan imaging to assess clogging of pervious concrete pavements in parking lots. *Journal of Environmental Management*, 95, 114–123.

Kim, J.Y. and Sansalone, J.J., 2008. Event-based size distributions of particulate matter transported during urban rainfall-runoff events Water Research, 42, 10–11, May 2008, 2756–2768.

Leming, M.L., Malcom, H.R., and Tennis, P.D., 2007. *Hydrologic design of pervious concrete*. Skokie, IL: Portland Cement Association.

Luck, J.D., *et al.*, 2006. Hydrologic properties of pervious concrete. *Transactions of the ASABE*, 49 (6), 1807–1813.

Maupin, G.W. Jr., 2000. Asphalt permeability testing in Virginia. *Transportation Research Record: Journal of the Transportation Research Board*, 1723, 83–91.

Maupin, G.W. Jr., 2001. Asphalt permeability testing: specimen preparation and testing variability. *Transportation Research Record: Journal of the Transportation Research Board*, 1767, 33–39.

Montes, F. and Haselbach, L., 2006. Measuring hydraulic conductivity in pervious concrete. *Environmental Engineering Science*, 23 (6), 960–969.

Montes, F., Valavala, S., and Haselbach, L., 2005. A new test method for porosity measurements of portland cement pervious concrete. *Journal of ASTM International*, 2 (1), 1–13.

Mulligan, A.M., 2005. *Attainable compressive strength of pervious concrete paving systems*. Master Thesis. University of Central Florida.

Neithalath, N., 2004. *Development and characterization of acoustically efficient cementations materials*. Thesis (phD). Purdue University.

Newman, A.P., *et al.*, 2004. Protecting groundwater with oil-retaining pervious pavements: historical perspectives, limitations and recent developments. *Quarterly Journal of Engineering Geology and Hydrogeology*, 37 (4), 283–291.

Nezu, I. and Nakagawa, H., 1993. *Turbulence in Open Channel Flows*. Balkema, Rotterdam, Netherlands: IAHR monograph series. A. A.

Nnadi, *et al.*, 2014a. An evaluation of enhanced geotextile layer in permeable pavement to improve stormwater infiltration and attenuation. *International Journal of Pavement Engineering*, 15 (10), 925–932.

Nnadi, *et al.*, 2014b. Geotextile incorporated permeable pavement system as potential source of irrigation water: effects of re-used water on the soil, plant growth and development. *CLEAN – Soil Air Water*, 42 (2), 125–132.

Nnadi, *et al.*, 2015. Stormwater harvesting for irrigation purposes: an investigation of chemical quality of water recycled in pervious pavement system. *Journal of Environmental Management*, 147 (2015), 246–256.

Pratt, C.J., Mantle, J.D.G., and Schofield, P.A., 1989. Urban stormwater reduction and quality improvement through the use of permeable pavements. *Water Science and Technology*, 21 (8/9), 769–778.

Pratt, C.J., Mantle, J.D.G., and Schofield, P.A., 1995. UK research into the performance of permeable pavement, reservoir structures in controlling stormwater discharge quantity and quality. *Water Science and Technology*, 32 (1), 63–69.

Pratt, C., Wilson, S., and Cooper, P., 2002. *Source control using constructed pervious surfaces: hydraulic, structural and water quality performance*

issues. London: Construction Industry and Research Association (CIRIA).

Prowell, B. and Dudley, M., 2002. Evaluation of measurement techniques for asphalt pavement density and permeability. *Transportation Research Record: Journal of the Transportation Research Board*, 1789, 36–45.

Rushton, B.T. and Bahk, B.M., 2001. Treatment of stormwater runoff from row crop farming in Ruskin, florida. *Water science and technology*, 44, 531–538.

Sañudo-Fontaneda, L.A., *et al.*, 2014. Infiltration behaviour of polymer-modified porous concrete and porous asphalt surfaces used in SuDS techniques. *CLEAN – Soil, Air, Water*, 42 (2), 139–145.

Schlüter, W. and Jefferies, C., 2002. Modelling the outflow from a porous pavement. *Urban Water*, 4 (3), 245–253.

Tennis, P.D., Leming, M.L., and Akers, D.J., 2004. *"Pervious Concrete Pavements", EB302, Portland Cement Association, Skokie, Illinois, and National Ready Mixed Concrete Association*. MD: Silver Spring.

White, H.E. and Walton, S.F., 1937. Particle packing and particle shape. *Journal of the American Ceramic Society*, 20, 155–166.

Williams, S.G., 2007. Sample size requirements for field permeability measurements of hot-mix asphalt pavements. *Transportation Research Record: Journal of the Transportation Research Board*, 2001, 56–62.

Xu, B.H. and Yu, A.B., 1997. Numerical simulation of the gas–solid flow in a fluidized bed by combining discrete particle method with computational fluid dynamics. Chemical Engineering Science, 52, 2786–2809.

AQ17